Reac Kinet Mech Cat (2012) 105:145–162
DOI 10.1007/s11144-011-0398-9

Oxidation of *tert*-butanethiol with air using Mo-containing hydrotalcite-like compounds and their derived mixed oxides as catalysts

Rodica Zăvoianu · Anca Cruceanu · Octavian Dumitru Pavel · Emilian Angelescu · Ana Paula Soares Dias · Ruxandra Bîrjega

Received: 2 June 2011 / Accepted: 31 October 2011 / Published online: 16 November 2011

Abstract This contribution presents several aspects concerning the production and characterization of hydrotalcite-like compounds containing Mo-species in the interlayer region (Mo-HT), the corresponding derived mixed oxides (Mo-CHT) and their catalytic activity in the demercaptanization of gasoline contaminated by *tert*-butanethiol. Mo-HT samples were obtained using two different molybdenum sources, e.g. Na_2MoO_4 or $(NH_4)_6Mo_7O_{24}$ and two preparation procedures: (i) ionic exchange and (ii) coprecipitation at pH 10 under high supersaturation. The derived mixed oxides were obtained by calcination at 450 °C during 24 h. The solids have been characterized by chemical analysis, TG/DTA, XRD, SEM–EDX, FTIR, DR-UV–Vis and Raman spectroscopy as well as determination of base sites. The specific area of the solids was determined using the BET method. The best catalysts were found to be those containing higher amounts of Mo species with tetrahedral coordination obtained by calcination of the Mo-HT precursors prepared at pH 10, either by ionic exchange or by co-precipitation using Na_2MoO_4 as a molybdenum source. Meanwhile, the catalysts containing mainly octahedrally coordinated Mo species (obtained from Mo-HT prepared at pH 10 using $(NH_4)_6Mo_7O_{24}{\cdot}6H_2O$ as molybdenum source) were characterized by a higher concentration of molybdenum species with octahedral coordination, lower number of base sites, smaller surface area, and a poor catalytic activity.

R. Zăvoianu (✉) · A. Cruceanu · O. D. Pavel · E. Angelescu
Department of Organic Chemistry, Biochemistry and Catalysis, Faculty of Chemistry, University of Bucharest, Bd. Regina Elisabeta, No. 4-12, S3, 030018 Bucharest, Romania
e-mail: rodicazavoianu@gmail.com
URL: http://www.unibuc.ro/prof/zavoianu_r/

A. P. S. Dias
ICEMS-UQUIMAF-GRECAT, Instituto Superior Técnico, Technical University of Lisbon, Av. Rovisco Pais, s/n, 1049-001 Lisbon, Portugal

R. Bîrjega
National Institute for Physics of Laser, Plasma and Radiation, Bucharest, Romania

Keywords Molybdenum mixed oxides · Demercaptanization · Hydrotalcite-like compounds · Tert-butanethiol oxidation

Introduction

The removal of sulfur from petroleum cuts is a priority in oil processing due to the exigencies imposed by environmental protection regulations. Among the sulfur-containing compounds, thiols are among the less desirable since they cause foul odor, deterioration of additives in finished products, poisoning of the catalysts used in oil processing and corrosion. Therefore, it is necessary to remove them, either by extraction or by their subsequent transforming to inoffensive alkyl disulfides. In the petroleum industry, such processes are usually called "sweetening". The most widely used sweetening process is Merox developed by UOP [1–3], which is based on the aerobic oxidation of alkane thiols to dialkyl disulfides at 25–40 °C, in alkaline environment (NaOH aqueous solution 10%wt.) in the presence of a soluble Co(II) complex catalyst with oxygen carrier properties (e.g. disodium Co(II)phtalocyanine-disulfonate), according to the reactions:

$$2RSH + 2NaOH \Leftrightarrow 2RSNa + 2H_2O \quad (1)$$

$$2RSNa + H_2O + [O] \rightarrow R - S - S - R + 2NaOH \quad (2)$$

$$2RSH + [O] \rightarrow R - S - S - R + H_2O \quad (3)$$

The addition of a base is necessary (pH = 9–9.5) because in the initial step a mercaptide ion has to be formed [4]. The sweetening process is highly efficient in demercaptanization since in the case of alkyl radicals R with more than 3 carbon atoms the disulfides which are not soluble in gasoline precipitate thus facilitating their complete removal from gasoline. However, the presence of the base solution raises serious problems due to its caustic character. Therefore, a special attention has been granted to the replacement of homogeneous sweetening catalysts with solid catalysts, such as those obtained by impregnation of an activated carbon with the Merox catalyst and the base compound. Several studies reported also the catalytic activity of metal complexes immobilized into layered double hydroxides (LDH) supports, especially Co(II)phtalocyanine-tetrasulfonate $[Co(PcTS]^{4-}$ for the auto-oxidation of thiols with O_2 [5–7]. The immobilization of the transition metal complex into LDH has three main effects on the catalytic behavior. First, the activity of Co complex is improved by heterogenization; second, the catalyst is more stable in time than the homogeneous homologue, and third, the LDH or the mixed oxides obtained from LDHs precursors not only act as a carrier but also as a solid base [8, 9], favoring the dissociation of thiols while playing a role similar to the one of the alkaline solutions used in homogeneous conditions.

The first report concerning the oxidation of thiols by molecular oxygen in the presence of a molybdenum compound entrapped in a LDH host (e.g. Zn–Al) was published by Corma et al. [10]. Layered double hydroxides defined by the general formula: $[M^{z+}_{1-x}M^{3+}_{x}(OH)_2]^{b+}[A^{n-}_{b/n}]$ m H_2O, (M = metal, A = interlayer anion, b = x or 2x−1, for z = 2 or 1), are anionic clays with laminar structure consisting

of positively charged brucite-type metal hydroxide layers with balancing anions and water molecules in the interlayer space. The most representative naturally occurring solid of this type is the mineral hydrotalcite (HT-CO_3^{2-}) having the formula $Mg_3Al(OH)_8(CO_3)_{0.5}{\cdot}2H_2O$ [11–16]. This type of solid is known to be a useful solid base catalyst. Its composition may be modified in order to obtain catalysts with both redox and base properties, yielding the so-called hydrotalcite-like compounds (HTlc). One of the methods used for the obtaining of HTlc is the replacement of Mg^{2+} or Al^{3+} cations from the brucite-type layer with other bivalent or trivalent transition metal cations having similar cationic radius and coordination preference. Another method implies the exchange of the carbonate anions from the structure with oxometallate or polyoxometallate anions. This method is applied for the modification with metals that are not compatible with the octahedral sites of the brucite-type sheet, such as Mo, or W [16–20]. HTlcs containing interlayer oxometallate or polyoxometallate anions can be used as precursors for obtaining new catalysts with outstanding properties due to the high dispersion and the possibility of migration and rearrangement of the active species [14, 16, 18]. Several Mo-containing HTlcs were proved to be active catalysts for different oxidation reactions such as selective olefin oxidation [21–23] or oxidative dehydrogenation of propane [24]. Most of the studies were directed towards HTlcs where Mo was present as heptamolybdate ($Mo_7O_{24}^{6-}$) species acting as pillars that expanded the distance between the brucite-type sheets [16, 17, 20–25]. Generally, these solids were prepared at low pH values in order to stabilize the $Mo_7O_{24}^{6-}$ anions.

Recently, several methods have been developed for producing hydrotalcite-like materials containing molybdate (MoO_4^{2-}) anions (Mo-HT), which are good catalysts for selective oxidations under mild conditions [26–28]. The dispersion, the accessibility and the coordination state of Mo in the active sites as well as its redox behavior are among the factors that influence strongly the catalytic activity. These characteristics are mainly determined by the preparation conditions (composition of the reaction mixture, pH, temperature, ageing treatment) used to obtain the catalyst.

Based on the above-mentioned facts, the aim of this contribution is to investigate the catalytic performances of Mo-containing HTlc (Mo-HT) and their derived mixed oxides (Mo-CHT) in the oxidation of *tert*-butanethiol (*t*-BuSH) with air. This test reaction has been selected since *t*-BuSH is one of the impurities difficult to be removed by catalytic sweetening from naphta gasoline. The influence of the preparation method as well as of the molybdenum source on the structural and physico-chemical properties of the solids is going to be analyzed in correlation with their catalytic activity.

Experimental

Preparation of the catalysts

Three Mo-containing HTlcs samples (Mo-HT) were obtained at constant pH 10 following two different procedures: ionic exchange (IE) without the presence of an organic swelling agent, or coprecipitation at high supersaturation using $Mg(NO_3)_2$,

$Al(NO_3)_3$ and two different molybdenum sources, Na_2MoO_4, and $(NH_4)_6Mo_7O_{24}$·NaOH and HNO_3 aqueous solutions (1.5 M) were used for pH adjustment. All reagents were purchased at high chemical purities (>98%) from Merck. Decarbonated distilled water was used for the preparation of the aqueous solutions. Both the ionic exchange and the direct synthesis were performed under inert atmosphere in order to avoid the contamination with CO_2.

For the preparation by ionic exchange according to the method previously developed by Kwon [29], an amount of Na_2MoO_4 solution (7.5×10^{-3} M) containing a number of MoO_4^{2-} anions equal to the half of the anionic exchange capacity (AEC) of a parent hydrotalcite $Mg_3Al(OH)_8(NO_3)\cdot2H_2O$ (HT-NO_3) synthesized by coprecipitation at constant pH = 10 and low supersaturation [11, 26] had been used. The pH was adjusted to 10 using a 1.5 M aqueous solution of NaOH.

The preparation by co-precipitation at pH = 10 and high supersaturation [11, 28], was performed by adding a Mg and Al-nitrates solution (1.5 M (Mg+Al), ratio Mg/Al = 3 initial pH = 4.5) with a constant flow rate of 1mL/min to a base solution (initial pH = 10.5) containing the appropriate amount of a molybdenum salt (e.g. Na_2MoO_4, or $(NH_4)_6Mo_7O_{24}$) aiming at a composition of Mg:Al:Mo = 3:1:0.25. The concentration of Mo in the aqueous base solution was 0.1 M. Aqueous NaOH solution (1.5 M) was used for the pH adjustment in the preparation with Na_2MoO_4 [28], while a NH_4OH solution (25%wt. NH_3) was used for the pH adjustment in the preparation with $(NH_4)_6Mo_7O_{24}$.

All the samples were submitted to an aging treatment at 65–70 °C during 18 h, followed by filtration, washing with decarbonated distilled water (up to pH = 7), and drying 18 h at 90 °C. Depending on the preparation procedure (PP) and the molybdenum source (S) used for obtaining the precursors, their names had been abbreviated as Mo-$HT_{PP\text{-}S}$: (i) Mo-$HT_{IE\text{-}Na2MoO4}$ (IE=ionic exchange at pH 10); (ii) Mo-$HT_{HS\text{-}Na2MoO4}$ (HS = direct synthesis at constant pH = 10 and high supersaturation and (iii) Mo-$HT_{HS\text{-}(NH4)6Mo7O24}$·

The mixed oxide catalysts (Mo-CHT) were obtained following the calcinations of the above-mentioned Mo-HT precursors under air-flow at 450 °C during 24 h. The names of these samples are defined by replacing the suffix HT with CHT in the name of the precursor, e.g. Mo-$CHT_{IE\text{-}Na2MoO4}$, Mo-$CHT_{HS\text{-}Na2MoO4}$ and Mo-$CHT_{HS\text{-}(NH4)6Mo7O24}$, respectively.

Characterization

The physico-chemical properties of the prepared solids were determined by chemical and TG-DTA analyses, XRD, BET, SEM–EDS, FTIR, DR-UV–Vis and Raman spectroscopy.

The metal content in the samples was determined by atomic absorption spectrometry (AAS) using a VARIAN AAS apparatus, while the carbon and nitrogen content of the samples was determined by elemental analysis performed with Carlo Erba automatic analyzer. The obtained results are presented in Table 1.

TG-DTA analyses were performed by heating the catalyst samples (50 mg) from 50 °C up to 800 °C (1 °C/min) under N_2 flow (50 mL/min) using SETARAM TG-DTA apparatus for recording TG and DTG curves and α-Al_2O_3 as standard.

Table 1 The chemical compositions of the catalysts

Samples	Mg wt. %	Al wt. %	Mo wt. %	N wt. %	C wt. %	Mg:Al:Mo Atomic ratio	H_2O* (wt. %)
Mo-$HT_{HS\text{-}Na2MoO4}$	17.4	7.2	2.8	2.6	0.1	2.68:1:0.11	12.0
Mo-$HT_{IE\text{-}Na2MoO4}$	22.8	9.2	2.7	1.0	0.2	2.75:1:0.08	12.3
Mo-$HT_{HS\text{-}(NH4)6Mo7O24}$	12.5	8.7	21.7	2.7	0.1	1.6:1:0.7	6.2
Mo-$CHT_{HS\text{-}Na2MoO4}$	28.5	11.3	4.4	–	0.2	2.8:1:0.1	8
Mo-$CHT_{IE\text{-}Na2MoO4}$	35.1	14.8	4.4	–	0.1	2.6:1:0.08	7.5
Mo-$CHT_{HS\text{-}(NH4)6Mo7O24}$	16.2	10.5	27.9	–	0.1	1.7:1:0.75	4.2

*As calculated considering the loss of weight determined by TG-DTA analysis in the range 105–200 °C [11]

The X-ray diffraction patterns of the samples were recorded using a DRON 3 diffractometer equipped with a graphite monochromator ($\lambda_{CuK\alpha}$ = 1.5418 Å). The samples were scanned from 7 to 70° (2θ) in steps of 0.05° with an acquisition time of 2 s at each point. The profile fitting calculations were performed using Jandel Scientific computer software and Voigt functions.

The catalysts were characterized by diffuse reflectance UV–VIS spectroscopy in the range 220–800 nm using SPECORD 80 UV–VIS spectrometer with an integration sphere coated with MgO taken as reference.

FTIR spectra in the range 400–4000 cm^{-1} were recorded on BioRad FTS 135 spectrometer using the KBr pellets technique. The concentration of the solid sample in the KBr matrix was 0.1 wt%.

Micro Raman spectra of the catalysts in the range 1424–196 cm^{-1} were recorded with 1 scan/8 s using SPEX 1877 triplemate spectrophotometer and the laser line 514.5360 nm as exciting radiation.

The specific surface area of the solids was determined by BET method from nitrogen adsorption–desorption isotherms at −196 °C using a Carlo-Erba instrument. Prior to the determination, the samples were degassed at 90 °C during 24 h under a pressure of 0.1 Pa.

The homogeneity of the samples was characterized by SEM–EDX using a HITACHI S2400 scanning electron microscope equipped with a RONTEC energy dispersive X-Ray high vacuum detector (W filament, E = 25 kV). The samples were analyzed from 15 mm working distance, with a resolution of 12 nm.

The surface base sites of the catalysts were determined on the basis of the irreversible adsorption of organic acids, such as acrylic acid, $pK_a = 4.2$ and phenol $pK_a = 9.9$, using a method that is suitable for both dried and calcined samples which was described in detail in a previous publication [30]. The amount of adsorbed phenol is related to the number of strong surface base sites while the amount of adsorbed acrylic acid is related to the total number of base sites. The number of weak base sites is given by the difference between the amount of adsorbed acrylic acid and the adsorbed phenol. Before base site measurements, all catalysts were thoroughly degassed under vacuum at room temperature.

Catalytic tests

In order to select the best catalysts, preliminary catalytic tests were performed by contacting synthetic samples of gasoline (100 mL) containing 128.5 ppm *t*-BuSH with the catalysts (1.3 g) under air flow (5 L/h) at ambient temperature and pressure, under continuous stirring during 4 h. For the series of catalysts presenting higher activity, the effects of the catalyst concentration, the air flow rate and the reaction time were also investigated. Another set of experiments aimed to investigate the resistance of the catalysts under operating conditions and the possibility of using them in six repeated reaction cycles (4 h each). The catalyst used in one reaction cycle was separated from the reaction mixture, washed with diethyl ether and dried under air flow during 1 h at 90 °C, before being introduced in the next cycle. The concentration of *t*-BuSH in the reaction mixture was determined by gas chromatography using a GC K072320 Thermo-Quest chromatograph equipped with a FID detector and a capillary column of 30 m length with DB5 stationary phase.

Results and discussions

The data presented in Table 1 show that both the ratio Mg/Al and the Mo uptake are different depending on the preparation conditions and the molybdenum source.

All the samples presented traces of carbon suggesting that carbonate is still present no matter what precautions are taken. For both Mo-HT samples prepared using Na_2MoO_4 as a molybdenum source either by ionic exchange or by co-precipitation at high supersaturation, the Mo-uptake was lower than the expected value considering the atomic ratio in the preparation mixture Mg:Al:Mo in the reaction mixture 3:1:0.25. For the sample prepared by ionic exchange this could be expected since the true exchange capacity of anionic clays (e. g. 1.0–1.5 meq g^{-1}) is usually much lower than the theoretical one (3.3 meq g^{-1} for HT-NO_3^-) [14, 16]. The atomic ratio Mg:Al was also slightly lower than 3, indicating that for these samples, there is probably a leaching of Mg during the washing stage. The differences in the Mg/Al ratios were also confirmed by the results of the XRD and SEM–EDX analyses (see Table 2). The chemical composition of the sample prepared using $(NH_4)_6Mo_7O_{24}$ as a molybdenum source was very different from that expected considering the composition of the reaction mixture, indicating that a high amount of molybdenum is incorporated in the structure in this case, but there is also a pronounced loss of Mg during the washing step since the ratio Mg/Al is much lower than 3 (e.g. 1.6). Compared to Mo-$HT_{HS\text{-}Na2MO4}$, Mo-$HT_{HS\text{-}(NH4)6Mo7O24}$ also presents a different behavior during thermal decomposition as it may be seen from the results of the thermal analysis presented in Fig. 1. Thus, the total loss of weight during the thermal decomposition of Mo-$HT_{HS\text{-}Na2MO4}$ was 39 wt% (typical for a hydrotalcite-like compound) whereas for Mo-$HT_{HS\text{-}(NH4)6Mo7O24}$, this loss of weight was only 23 wt%, indicating a higher thermal stability. Mo-$HT_{HS\text{-}Na2MO4}$ which has a low concentration of Mo presents two weight losses accompanied by strong endothermic effects at 235 and 419 °C respectively, while the sample

Table 2 Results of XRD, SEM–EDX and BET analyses for Mo-HT samples

Mo-HT Samples	Lattice parameters		IFS	$\frac{I_{003}}{I_{110}}$	Mg/Al	Mg/Al/Mo	D_{003}[b]	D-$_{110}$[b]	S_{sp}
	a (Å)	*c* (Å)	(Å)		(XRD)[a]	(SEM–EDX)	(Å)	(Å)	(m^2/g)
Mo-$HT_{IE\text{-}Na2MoO4}$	3.060	23.521	2.93	5.98	2.75	2.72/1/0.11	78	166	58
Mo-$HT_{IE\text{-}Na2MoO4}$	3.060	23.521	2.93	5.98	2.75	2.72/1/0.11	78	166	58
Mo-$HT_{HS\text{-}Na2MoO4}$	3.058	23.310	2.97	7.53	2.71	2.7/1/0.12	119	182	47
[C]Mo-$HT_{HS\text{-}(NH4)6Mo7O24}$	–	–	–	–	–	1.72/1/0.9 (1.2/0/0.5)*	–	–	35
Reference material $Mg_3Al\text{-}CO_3^{2-}$	3.065	23.716	3.10	8.29	3.00	3/1/0	77	145	65

*Traces in the less homogeneous samples

[a] The ratios Mg/Al were calculated using the values of the lattice constant *a*, and Vegard's law [11]

[b] D_{003} (Å) and D_{110} (Å) are the sizes of the crystals determined using Debye-Sherrer formula for two directions perpendicular to the planes (003) and (110), respectively

[c] For Mo-$HT_{HS\text{-}(NH4)6Mo7O24}$ due to the low crystallinity the values of the lattice parameters have not been calculated

Mo-$HT_{HS\text{-}(NH4)6Mo7O24}$, which has a high concentration of Mo, shows four stages of weight loss accompanied by endothermic effects at 177, 445, 526, and 571 °C. The effects noticed at temperatures higher than 500 °C are ascribed to the thermal decomposition of the paramolybdate anions [31].

The calcined samples Mo-CHT have higher Mg, Al, Mo concentrations since the nitrate anions and most of the hydroxyl groups are lost during calcination. However, since calcination takes place under air flow, traces of carbonate are also found.

The XRD patterns of Mo-HT samples prepared by ionic exchange or co-precipitation at high supersaturation using Na_2MoO_4 as a molybdenum source (Fig. 2Ia, b) exhibit a typical hydrotalcite structure with sharp and symmetric reflections for (003), (006), (110) and (113) planes and broad asymmetric peaks for (012), (015) and (018) planes (JCPDS 70-2151) [11]. The reflections were indexed in a hexagonal lattice with R3m rhombohedral symmetry. The cell parameters are given by $a = 2 \times d_{110}$ and $c = \frac{3}{2} \times (d_{003} + 2\, d_{006})$. The interlayer free spacing (IFS) was calculated by subtracting the brucite sheet thickness (e.g. 4.8 Å as reported by Miyata [32]) from $\frac{c}{3}$ values. These samples have a homogeneous composition as indicated by SEM–EDX analysis. The basal space peaks are very sharp and intense revealing high stacking order along *c* axis due to a more compact orientation of the anions which are mainly NO_3^-. The (*0kl*) peaks are less asymmetric compared to those of the reference pattern of the natural mineral HT-CO_3^{2-}, showing less turbostratic disorder effects. In their case the decrease of the Mg/Al ratio compared to the standard HT-CO_3^{2-} is accompanied by the decrease of *c* parameter and consequently of the IFS. This fact indicates stronger electrostatic interactions between layer and interlayer anions due to the higher amount of Al^{3+} in the brucite sheet.

The diffraction pattern of Mo-$HT_{HS\text{-}(NH4)6Mo7O24}$ (Fig. 2Ic) shows a considerably disordered structure with broader and less defined peaks. The maximum of the

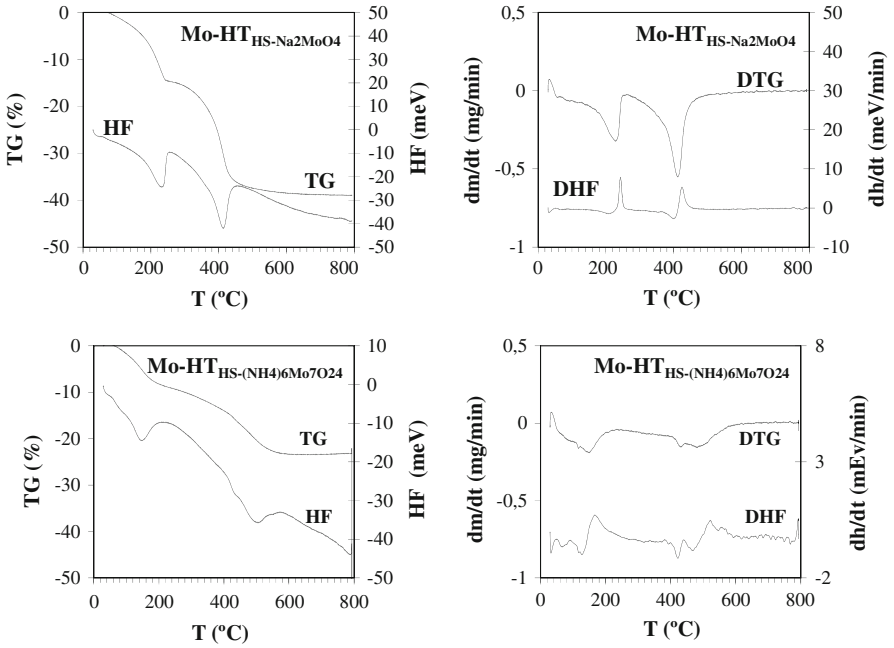

Fig. 1 TG and HF profiles for Mo-$HT_{HS\text{-}Na2MoO4}$, and Mo-$HT_{HS\text{-}(NH4)6Mo7O24}$

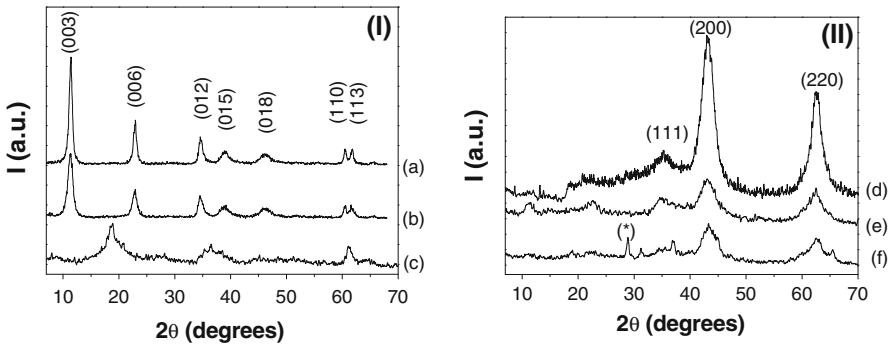

Fig. 2 XRD patterns of the catalysts: (I) Mo-HT precursors: *a* Mo-$HT_{HS\text{-}Na2MoO4}$, *b* Mo-$HT_{IE\text{-}Na2MoO4}$, *c* Mo-$HT_{HS\text{-}(NH4)6Mo7O24}$, (II) Mo-CHT mixed oxides: *d* Mo-$CHT_{HS\text{-}Na2MoO4}$, *e* Mo-$CHT_{IE\text{-}Na2MoO4}$, *f* Mo-$CHT_{HS\text{-}(NH4)6Mo7O24}$, * diffraction lines of Mo compounds impurities

reflection corresponding to (003) plane shifted to lower values of 2θ suggests the location of the paramolybdate species in the interlayer. The significant broadening of the second diffraction line (006), which is also shifted to lower values of 2θ, highlights the disorder in the stacking of the planes (00l) due to the presence of the Mo species similarly to the phenomenon reported in the case of the intercalation of metavanadate species [33, 34]. The wide basal peaks and the broad diffraction band corresponding to the (110) plane suggest the presence of small crystallites.

Normally, the smaller size of the crystallites would lead to a larger surface area. However as it may be seen from Table 2, this sample has the lowest surface area. This fact was also confirmed by the SEM microphotographs presented in Fig. 3 where it may be seen that at the same magnification level (e.g. 2700), the particles of Mo-$HT_{HS\text{-}(NH4)6Mo7O24}$ exhibit a quasi-flat surface with small excrescences while the particles of Mo-$HT_{HS\text{-}Na2MoO4}$, which has a well-defined diffraction pattern, show a porous layered structure. Therefore it may be assumed that the poor crystallinity of Mo-$HT_{HS\text{-}(NH4)6Mo7O24}$ may be due to the presence of a compact amorphous phase covered with small crystallites. The less homogeneous composition of Mo-$HT_{HS\text{-}(NH4)6Mo7O24}$ was also revealed by the results of SEM–EDX analysis presented in Table 2.

The XRD patterns of Mo-$CHT_{IE\text{-}Na2MoO4}$ and Mo-$CHT_{HS\text{-}Na2MoO4}$ (Fig. 2IId, e) present the typical features of Mg(Al)O mixed oxide with periclase structure (a = 4.184 and 4.193Å, respectively) and no traces of polymolybdate species have been noticed. Meanwhile, the pattern of Mo-$CHT_{HS\text{-}(NH4)6Mo7O24}$ (Fig. 2IIf) shows a high amount of amorphous phase with several diffraction lines corresponding to molybdenum compounds. The unit cell parameter and the mean crystallite size were evaluated assuming a Voigt profile function. The mean crystallite size was determined using the Debye–Scherrer formula:

$$D = (k * \lambda / \beta \cos\theta) \quad (4)$$

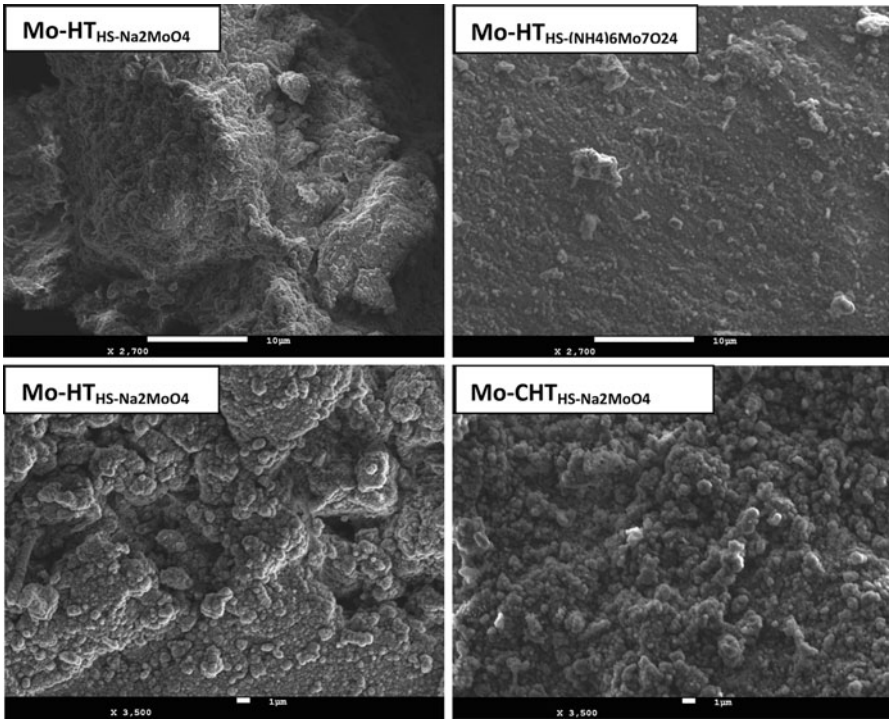

Fig. 3 SEM microphotographs of Mo-$HT_{HS\text{-}Na2MoO4}$, Mo-$HT_{HS\text{-}(NH4)6Mo7O24}$ and Mo-$CHT_{HS\text{-}Na2MoO4}$

where θ is the Bragg angle, β is the fullwidth at half maximum of the peak corrected by the instrumental broadness, λ is the X-ray wavelength ($\lambda_{CuK\alpha}$ = 1.5418 Å) and k is the structural factor (taken as 0.9 for the cubic structure of MgO). The mean crystallite size was calculated as an average value given by the FWHM of (200) and (220) peaks. The results are presented in Table 3.

The surface areas of the calcined samples presented in Table 3 are larger than those corresponding to the dried precursors, while respecting the same variation order (e.g. the largest surface area is exhibited by the samples prepared by ionic exchange with Na_2MoO_4, followed by the sample prepared by co-precipitation at high supersaturation with Na_2MoO_4 and the lowest surface area is characteristic of the sample prepared at high supersaturation with $(NH_4)_6Mo_7O_{24}$). The effect of calcination on the surface modification is illustrated by the SEM microphotographs in Fig. 3, where it may be seen that at the same magnification level (e.g. 3500) the dimensions of the particles in Mo-$CHT_{HS\text{-}Na2MoO4}$ are smaller than those in Mo-$HT_{HS\text{-}Na2MoO4}$.

The FTIR spectra of the molybdenum containing catalysts are presented in Fig. 4.

The FTIR spectra of the Mo-HT samples (Fig. 4a, c, e) show broad adsorption bands suggesting a high disorder of the molecules in the galleries. Meanwhile, the band corresponding to Mo–O–Mo stretching vibrations at 665 cm^{-1}, the one related to MoO_4^{2-} at 856 cm^{-1} and the band for Mo=O stretching at 914 cm^{-1} [25, 35] appear in the same region as those characteristic for a typical HT structure. Therefore, due to the overlapping, it is difficult to comment the nature of Mo species in the modified HTlcs. The most significant difference between the FTIR spectra of the samples Mo-$HT_{HS\text{-}Na2MOO4}$ and Mo-$HT_{HS\text{-}(NH4)6Mo7O24}$ is the higher intensity of the peak at 1400 cm^{-1} ascribed to the presence of NO_3^- anions [36] in the spectrum of Mo-$HT_{HS\text{-}Na2MOO4}$. This band overlaps the one characteristic for the vibrations of CO_3^{2-}, which is present in traces as it was shown by the results of the chemical analysis presented in Table 1. The effect of the ionic exchange for the sample Mo-$HT_{IE\text{-}Na2MoO4}$ is noticed due to the lowering of the band corresponding to NO_3^-vibrations compared to the band in the spectrum of Mo-$HT_{HS\text{-}Na2MoO4}$.

In the FTIR spectra of the calcined samples (Fig. 4b, d, f) the decrease of the intensity of the band corresponding to the hydroxyl groups at 3460 cm^{-1} compared to the spectra of Mo-HT samples was noticed. The FTIR spectrum of Mo-$CHT_{HS\text{-}(NH4)6Mo7O24}$ indicates that this sample has a lower amount of hydroxilic groups and a higher amount of Mo incorporated compared to Mo-$CHT_{HS\text{-}Na2MoO4}$, whose

Table 3 Results of XRD, SEM–EDX and BET analyses for Mo-CHT samples

Sample	Unit cell parameter (a) (Å)	Mean crystallite size (Å)	Mg/Al/Mo (SEM–EDX)	S_{BET} (m^2/g)
Mo-$CHT_{HS\text{-}Na2MoO4}$	4.193	36	2.81/1/0.09	100
Mo-$CHT_{IE\text{-}Na2MoO4}$	4.184	38	2.65/1/0.1	150
Mo-$CHT_{HS\text{-}(NH4)6Mo7O24}$	4.171	32	1.7/1/0.9	82

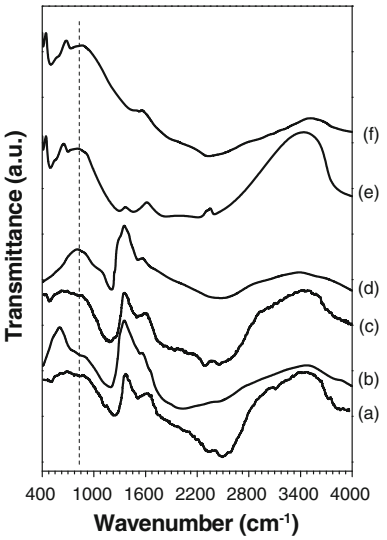

Fig. 4 FTIR spectra of Mo-containing samples (*a* Mo-$HT_{HS\text{-}Na2MoO4}$, *b* Mo-$CHT_{HS\text{-}Na2MoO4}$, *c* Mo-$HT_{IE\text{-}Na2MoO4}$, *d* Mo-$CHT_{IE\text{-}Na2MoO4}$, *e* Mo-$HT_{HS\text{-}(NH4)6Mo7O24}$, *f* Mo-$CHT_{HS\text{-}(NH4)6Mo7O24}$, —856 cm^{-1})

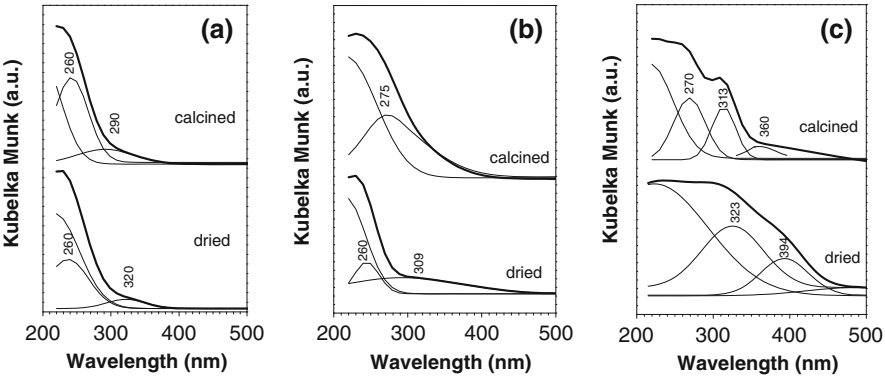

Fig. 5 DR-UV–Vis spectra of Mo-containing samples **a** dried—Mo-$HT_{HS\text{-}Na2MoO4}$; calcined—Mo-$CHT_{HS\text{-}Na2MoO4}$; **b** dried—Mo-$HT_{IE\text{-}Na2MoO4}$, calcined—Mo-$CHT_{IE\text{-}Na2MoO4}$; **c** dried—Mo-$HT_{HS\text{-}(NH4)6Mo7O24}$, calcined—Mo-$CHT_{HS\text{-}(NH4)6Mo7O24}$

spectrum displays higher intensity bands corresponding to hydroxyl groups while the bands corresponding to Mo–O bonds are noticed as shoulders.

Fig. 5 displays the DR-UV–Vis spectra of the Mo containing catalysts in the region 220–500 nm where the absorption bands characteristics to Mo species appear.

According to literature data, the isolated MoO_4^{2-} species with Mo in tetrahedral coordination present absorption bands in the region 260–280 nm, while the bands in the region 300–320 nm are due to $Mo_7O_{24}^{6-}$ and isolated MoO_3 species with Mo^{6+} in octahedral coordination [37, 38]. As it may be seen from Fig. 5, all the samples contain both Mo in tetrahedral and octahedral coordination. However, in the samples prepared with Na_2MoO_4, (Fig. 5a, b) the amounts of tetrahedrally

coordinated species are prevailing whereas in the samples prepared from $(NH_4)_6Mo_7O_{24}$ (Fig. 5c) the octahedrally coordinated species prevail.

The results obtained by DR-UV–Vis were confirmed by those of Raman spectroscopy analysis illustrated by the spectra presented in Fig. 6.

The Raman spectra revealed the presence of the most intense absorption band corresponding to Mo–O symmetrical stretching vibration in MoO_4^{2-} at 896 cm^{-1} and the one corresponding to δ(Mo=O) in MoO_4^{2-} at 320 cm^{-1} [21, 26] in all the calcined samples, even if in the case of Mo-$CHT_{HS\text{-}(NH4)6Mo7O24}$ (Fig. 6c) the intensity of these bands was much lower. The bands characteristic for $Mo_7O_{24}^{6-}$ at 940 cm^{-1} (highest intensity), 564 and 219 cm^{-1} (Mo–O-Mo ν and δ vibrations) and 340 cm^{-1} (δ(Mo=O)) [39] could be discerned clearly in the spectrum of Mo-$CHT_{HS\text{-}(NH4)6Mo7O24}$, while in the spectra of Mo-$CHT_{IE\text{-}Na2MoO4}$ and Mo-$CHT_{HS\text{-}Na2MoO4}$ (Fig. 6a, b), only the band at 940 cm^{-1} could be noticed as a shoulder.

The results of the preliminary catalytic tests (Fig. 7) performed by contacting the catalysts with synthetic samples of gasoline contaminated with 128.5 ppm *t*-BuSH under air flow at ambient temperature and pressure showed that for all Mo-HT samples the conversions of *t*-BuSH were lower by 10–25% than those obtained in the presence of the corresponding derived mixed oxides Mo-CHT. At a first glance, this fact should be explainable by the increase of the surface area in the mixed oxide samples (see Table 3) compared to the hydrotalcite-type precursors (see Table 2).

However, it was surprising to notice that the lowest conversion level was obtained in the presence of the samples containing the highest concentration of Mo, e.g. Mo-$HT_{HS\text{-}(NH4)6Mo27O24}$ and Mo-$CHT_{HS\text{-}(NH4)6Mo27O24}$, which yielded only 15 and 24% conversion of *t*-BuSH. These conversion values are less than half of the conversions reached with the catalysts prepared using Na_2MoO_4 as a molybdenum source, which have a concentration of Mo sites that is 6-8 times lower than in Mo-$HT_{HS\text{-}(NH4)6Mo27O24}$ and Mo-$CHT_{HS\text{-}(NH4)6Mo27O24}$ samples. Meanwhile, the specific surface areas of these catalysts (35 and 82 m^2/g, respectively) are only approximately ¼ lower than those of the samples Mo-$HT_{HS\text{-}Na2MoO4}$ and Mo-$CHT_{HS\text{-}Na2MoO4}$. One fact revealed clearly by the characterization of the samples that might be related to the poor catalytic activity of Mo-$HT_{HS\text{-}(NH4)6Mo27O24}$ and Mo-$CHT_{HS\text{-}(NH4)6Mo27O24}$ could be the low amount of Mo species with tetrahedral coordination included in these samples. Another fact that could be accounted as responsible for

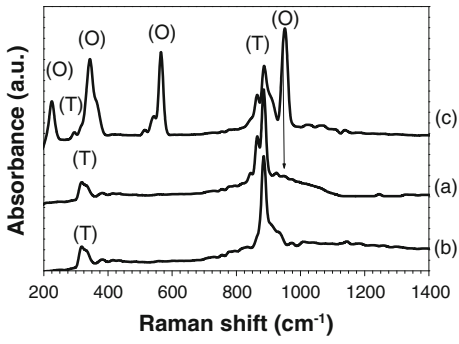

Fig. 6 Raman spectra of Mo-CHT samples (*a* Mo-$CHT_{HS\text{-}Na2MoO4}$, *b* Mo-$CHT_{IE\text{-}Na2MoO4}$, *c* Mo-$CHT_{HS\text{-}(NH4)6Mo7O24}$, *T* tetragonal, *O* octahedral)

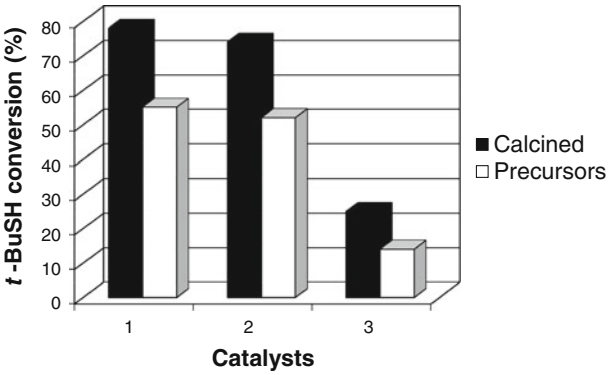

Fig. 7 Comparison of the catalytic activities of precursors and calcined samples, air flow 5 L/h, 1.3 g catalyst, 100 mL gasoline with $C_{o\ t\text{-BuSH}} = 128.5$ ppm, 4 h reaction time. Precursors: *1* $MoHT_{IE\text{-}Na2MoO4}$; *2* $MoHT_{HS\text{-}Na2MoO4}$; *3* $MoHT_{HS\text{-}(NH4)6Mo27O24}$; Calcined: *1* $MoCHT_{IE\text{-}Na2MoO4}$; *2* $MoHT_{HS\text{-}Na2MoO4}$; *3* $MoHT_{HS\text{-}(NH4)6Mo27O24}$

their low activity would be a lower basicity of the surface which would lead to an inefficient activation of the alkanethyol reactant.

In order to confirm this supposition, the surface base sites of the catalysts was determined using a method based on the irreversible adsorption of organic acids, (acrylic acid, $pK_a = 4.2$ and phenol $pK_a = 9.9$) that is suitable for both dried and calcined samples [30]. The results presented in Table 4, show that undoubtedly the samples prepared with $(NH_4)_6Mo_7O_{24}$ have the lowest number of base sites, while the samples prepared either by ionic exchange or by co-precipitation with Na_2MoO_4 exhibit higher basicity. The values of the base sites numbers obtained for $Mo\text{-}HT_{IE\text{-}Na2MoO4}$ and $Mo\text{-}HT_{HS\text{-}Na2MoO4}$ are slightly lower than those characteristic to $HT\text{-}CO_3^{2-}$ (e.g. 6.47 mmol weak base sites/g and 0.26 mmol strong base sites/g [30]). Meanwhile, those obtained for the corresponding Mo-CHT samples are also just a little bit lower than those obtained for the mixed oxide CHT obtained from $HT\text{-}CO_3^{2-}$ precursor (e.g. 7.98 mmol weak base sites/g and 0.38 mmol strong base sites/g [30]).

Based on the above mentioned aspects it may be concluded that both the presence of the base sites as well as the presence of tetrahedral coordinated Mo species are required for the oxidation of *t*-BuSH. In the first stage, the *t*-BuSH molecule is activated by dissociation in the presence of the base sites of the solid. In the case of Mo-HT samples, the OH^- ions in the interlayer act as Brønsted base sites with a stronger basicity than MoO_4^{2-}, or $Mo_7O_{24}^{6-}$ and NO_3^- ions. In the case of Mo-CHT samples, the base surface sites consist of OH^- groups (low strength), M–O pairs (medium strength) and O^{2-} (strong) [40]. After the dissociation the *t*-$BuSH^-$ anion is adsorbed preferentially on tetracoordinated Mo^{6+} sites due to the fact that these ones can undergo easily a change in their coordination state. The Mo^{6+} is then reduced to Mo^{5+} and a radical *t*-BuSH* is generated. Two *t*-BuSH* radicals will combine to generate the dialkyl disulfide *t*-Bu-S–S-*t*-Bu while the reoxidation of the Mo sites will be ensured by the oxygen in the air flow. Further studies using XPS

Table 4 Surface base sites of the samples determined in fully hydrated conditions and by irreversible adsorption of organic acids

Sample	Base properties in fully hydrated conditions* (pH)	Base sites (mmol/g)	
		Weak base sites[a]	Strong base sites[b]
Mo-$HT_{IE\text{-}Na2MoO4}$	10	5.85	0.20
Mo-$HT_{HS\text{-}Na2MoO4}$	9.8	5.79	0.17
Mo-$HT_{HS\text{-}(NH4)6Mo7O24}$	7.2	2.72	0.05
Mo-$CHT_{IE\text{-}Na2MoO4}$	10.2	6.88	0.32
Mo-$CHT_{HS\text{-}Na2MoO4}$	10	6.71	0.26
Mo-$CHT_{HS\text{-}(NH4)6Mo7O24}$	7.5	3.34	0.10

*Determined by pH measurement of a suspension containing 1.5 g solid sample in 100 mL distilled water

[a] (moles of acrylic acid–moles of phenol) adsorbed/gram of catalyst

[b] moles of phenol adsorbed/gram of catalyst

measurements in order to confirm the proposed mechanism are going to be performed in the near future.

Since the calcined catalysts exhibited better catalytic activity, they were selected for further testing in order to establish the optimal reaction conditions. In a first series of tests, the influence of the concentration of catalyst in the reaction mixture has been investigated. The results presented in Fig. 8a show that, for all catalysts, the conversion of *t*-BuSH increases almost linearly when the concentration of catalyst in the reaction mixture varies from 0.8 up to 1.3 wt%. A further increase of the concentration of the catalyst does not lead to significant increases of the conversion. The highest level of the conversion (80%) is reached with the catalyst Mo-$CHT_{IE\text{-}Na2MoO4}$. For the less active catalyst, the conversion does not exceed 30% even at the highest concentration of solid in the reaction mixture. Taking these results into account, it may be concluded that a concentration of 1.5 wt% catalyst in the reaction mixture would be preferable for obtaining high conversion levels.

In the second series of tests, the effect of the air flow rate on the conversion of *t*-BuSH was investigated using the previously selected concentration of catalyst in the reaction mixture. The results plotted in Fig. 8b show that the conversion of *t*-BuSH increases sharply when the air flow rate varies from 1 up to 5 L/h, while the further increase of the air flow rate does not lead to significant improvements. Therefore it may be considered that an air flow rate of 6 L/h would be optimal for further experiments.

In the third series of tests, the effect of the reaction time on the catalytic activity was investigated using the optimal concentration of catalyst in the reaction mixture and the optimal air flow rate selected. The results plotted in Fig. 8c show that after 4 h reaction time, almost stable values of the conversion of *t*-BuSH are obtained and there is no decrease of the catalytic activity during 10 h. The fact that the total conversion of this reactant cannot be reached even when the reaction time is extended may be a consequence of two factors: (i) the lower reactivity of *t*-BuSH

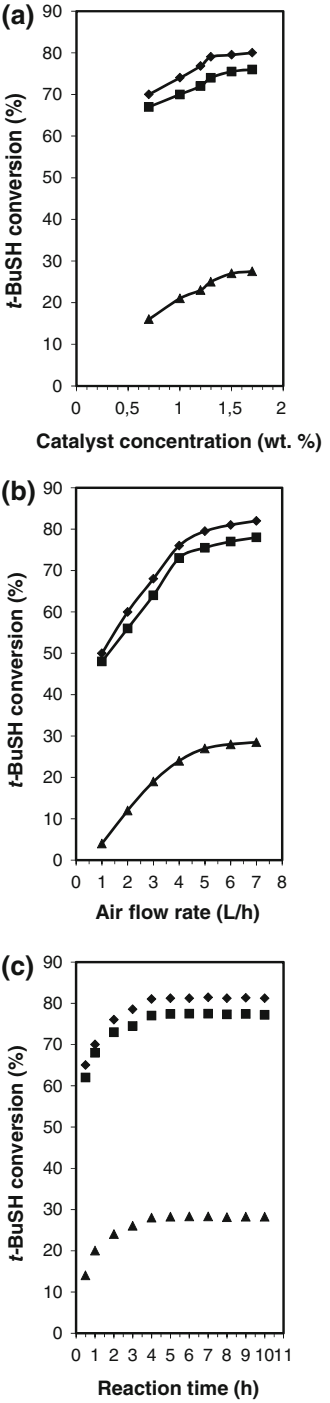

Fig. 8 Results of catalytic tests for *t*-BuSH oxidation using 100 mL gasoline with $C_{o\ t\text{-BuSH}} = 128.5$ppm and Mo-containing catalysts (*filled square* Mo-$CHT_{HS\text{-}Na2MoO4}$, *filled diamond* Mo-$CHT_{IE\text{-}Na2MoO4}$, *filled triangle* Mo-$CHT_{HS\text{-}(NH4)6Mo7O24}$); **a** effect of catalyst concentration (air flow rate 5 L/h, 4 h reaction time); **b** effect of air flow rate (concentration of catalyst 1.5 wt%, 4 h reaction time); **c** effect of reaction time (concentration of catalyst 1.5 wt%, air flow rate 6 L/h)

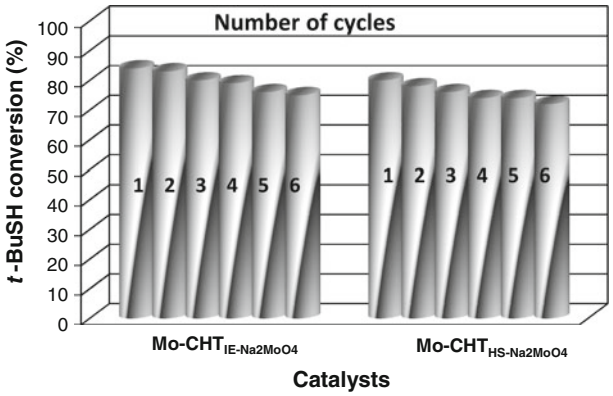

Fig. 9 Results of catalytic tests for *t*-BuSH oxidation, air flow rate 6 L/h, concentration of catalyst 1.5 wt%, 100 mL gasoline with $C_{o\text{-}BuSH} = 128.5$ ppm, repeated reaction cycles

compared to the other light alkane thiols due to its molecular structure, (ii) the partial screening of the active sites of the catalyst by the reaction products (disulfide and water) during the process.

The fourth set of experiments aimed to investigate the resistance of the catalysts under operating conditions and the possibility of using them in repeated reaction cycles (4 h each). The results (Fig. 9) indicate that the catalytic activity decreases gradually with about 8% after six reaction cycles. It may be supposed that the deactivation occurs due to the adsorption of the reaction products on the surface of the solids, even though the catalysts had been thoroughly washed with diethyl ether in order to remove the adsorbed disulfide before being used in the next cycle.

The gasoline recovered after six reaction cycles was collected and submitted to ICP-OES analysis (ASTM-E 1479-92) in order to examine the leaching of Mo, Mg, and Al. For both catalysts Mo-$CHT_{IE\text{-}Na2MoO4}$ and Mo-$CHT_{HS\text{-}Na2MoO4}$, the concentrations of Mg, Al and Mo in the recovered liquid phase were lower than the detection limits (e.g. $Mg < 0.1$ ppm, $Al < 0.02$ ppm and $Mo < 0.05$ ppm), suggesting that leaching did not occur under reaction conditions.

Conclusions

The obtained results showed that the higher activity towards the oxidation of *t*-BuSH is strongly related to two factors: (i) the presence of tetrahedral coordinated Mo species well dispersed in the structure of the base solid, and (ii) the amount of base sites in the solid. The preparation of Mo-HT solids at pH 10, using Na_2MoO_4 as molybdenum source allows the obtaining of crystalline materials with relatively high basicity and fine dispersion of molybdate species. These solids exhibit the best catalytic activity for the oxidation of *t*-BuSH (e.g. about 80% conversions). The preparation of Mo-HT solids at pH 10, using $(NH_4)_6Mo_7O_{24}$ as molybdenum source and NH_4OH for pH adjustment, lead to less crystalline solids with smaller surface

area and lower basicity. In these solids, which had the lowest catalytic activity, Mo was present mainly as octahedral coordinated species.

Acknowledgments The Romanian authors express their gratitude to the Romanian National Agency for Scientific Research for financial support through grant 71-043 ECOPAM under the framework of PNCDI Partenerships program.

References

1. Alcaraz JJ, Arena BJ, Gillespie RD, Holmgren JS (1998) Solid base catalysts for mercaptan oxidation. Catal Today 43:89–99
2. Jiang DE, Zhao BY, Xie YC, Pan GC, Ran GP, Min E (2001) Structure and basicity of gamma-Al_2O_3-supported MgO and its application to mercaptan oxidation. Appl Catal A-Gen 219:69–78
3. Chatti I, Ghorbel A, Grange P, Colin JM (2002) Oxidation of mercaptans in light oil sweetening by cobalt(II) phthalocyanine-hydrotalcite catalysts. Catal Today 75:113–117
4. Angelescu E, Cruceanu A, Zavoianu R, Angelescu A (2006) Transitional metals sulphonated phtalocyanines, catalysts for the demercaptanization of gasolines. Rev Chim-Bucharest 57:85–90
5. Iliev VI, Ileva AI, Dimitrov LD (1995) Catalytic oxidation of 2-mercaptoethanol by cobalt(II)-phthalocyanine complexes intercalated in layered double hydroxides. Appl Catal A-Gen 126: 333–340
6. Iliev V (1993) Catalytic oxidation of mercaptans by charcoal-supported sterically hindered cobalt (II)-phthalocyanines. J Mol Catal 85:L269–L273
7. Buck T, Bohlen H, Wohrle D, Schulz-Ekloff G, Andreev A (1993) Influence of substituents and ligands of various cobalt (II) porphyrin derivatives coordinately bonded to silica on the oxidation of mercaptan. J Mol Catal 80:253–267
8. De Vos DE, Jacobs PA (2001) Chapter 20 Zeolite-based supramolecular assemblies. In: van Bekkum H, Flanigen EM, Jacobs PA, Jansen JC (eds) Introduction to Zeolite Science and Practice, Stud Surf Sci Catal, vol 137. Elsevier, Amsterdam, pp 957–985
9. Perez-Bernal ME, Ruano-Casero R, Pinnavaia TJ (1991) Catalytic autoxidation of 1-decanethiol by cobalt(II)phthalocyaninetetrasulfonate intercalated in a layered double hydroxide. Catal Lett 11:55–61
10. Corma A, Fornes V, Rey F, Cervilla A, Llopis E, Ribera A (1995) Catalytic air oxidation of thyols mediated at a $Mo(VI)O^{-2}$ complex center intercalated in a Zn(II)-Al(III) layered double hydroxyde host. J Catal 152:237–242
11. Cavani F, Trifiro F, Vaccari A (1991) Hydrotalcite-type anionic clays: preparation, properties and applications. Catal Today 11:173–301
12. Albertazzi S, Basile F, Vaccari A (2004) Catalytic Properties of Hydrotalcite-Type Anionic Clays. In: Wypych F, Satyanarayana KG (eds) Clay Surfaces Fundamental and Applications, Interface Science and Technology, vol 1. Elsevier, london, pp 497–546
13. Basile F, Vaccari A (2001) Chapter 10. In: Rives V (ed) Layered double hydroxides: present and future. Nova Science Publisher, New York
14. Vaccari A (1999) Clays and catalysis: a promising future. Appl Clay Sci 14:161–198
15. Cheng S (1999) From layer compounds to catalytic materials. Catal Today 49:303–312
16. Trifiro F, Vaccari A (1996) Hydrotalcite-like Anionic Clays (Layered Double Hydroxides) in Comprehensive Supramolecular Chemistry. In: Alberti G, Bein T (eds) Solid-State Supramolecular Chemistry: two and Three-Dimensional Inorganic Networks, vol 7. Elsevier Science Ltd, Pergamon, pp 251–291
17. Drezdon MA (1988) Synthesis of Isopolymetalate-Pillared Hydrotalcite via Organic-Anion-Pillared Precursors. Inorg Chem 27:4628–4632
18. Rives V, Ulibarri MA (1999) Layered double hydroxides (LDH) intercalated with metal coordination compounds and oxometalates. Coord Chem Rev 181:61–120
19. Ulibarri MA, Hermosin MC (2001) Chapter 9. In: Rives V (ed) Layered double hydroxides: present and future. Nova Science Publisher, New York
20. Drezdon MA (1988) Pillared hydrotalcites. US Patent 4,774,212 Assignee to Amoco Corporation, 27 Sept 1998

21. Gardner E, Pinnavaia TJ (1998) On the nature of selective olefin oxidation catalysts derived from molybdate- and tungstate-intercalated layered double hydroxides. Appl Catal A-Gen 167:65–74
22. Pinnavaia TJ, Chibwe M, Constantino VRL, Yun SK (1995) Organic-chemical conversions catalyzed by intercalated layered double hydroxides (LDHS). Appl Clay Sci 10:117–129
23. Tatsumi T, Yamamoto K, Tajima H, Tominga H (1992) Shape selective epoxidation of alkenes catalyzed by polyoxometalate-intercalated hydrotalcite. Chem Lett 5:815–818
24. Mitchell PCH, Wass SA (2002) Propane dehydrogenation over molybdenum hydrotalcite catalysts. Appl Catal A-Gen 225:153–165
25. Malherbe F, Depège C, Forano C, Besse JP, Atkins MP, Sharma B, Wade SR (1998) Alkoxylation reaction catalysed by layered double hydroxides. Appl Clay Sci 13:451–466
26. van Laar FMPR, De Vos DE, Pierard F, Kirsch De-Mesmaeker A, Fiermans L, Jacobs PA (2001) Generation of singlet molecular oxygen from H_2O_2 with molybdate-exchanged layered double hydroxides: effects of catalyst composition and reaction conditions. J Catal 197:139–150
27. van Laar FMPR, De Vos DE, Vanoppen D, Sels B, Jacobs PA (1998) Heterogeneous molybdate catalysts for the generation of singlet molecular oxygen ($^1\Delta_g$) from H_2O_2. Chem Commun 267–268
28. Zavoianu R, Birjega R, Pavel OD, Cruceanu A, Alifanti M (2005) Hydrotalcite like compounds with low Mo-loading active catalysts for selective oxidation of cyclohexene with hydrogen peroxide. Appl Catal A-Gen 286:211–220
29. Kwon T, Tsigdinos GA, Pinnavaia TJ (1988) Pillaring of layered double hydroxides (LDH's) by polyoxometalate anions. J Am Chem Soc 110:3653–3654
30. Ionescu R, Birjega R, Angelescu E, Pavel OD, Zavoianu R (2010) Epoxidation of cyclohexene with H_2O_2 and acetonitrile catalyzed by Mg–Al hydrotalcite and cobalt modified hydrotalcites. Catal Lett 34:309–317
31. Rives V (2002) Characterisation of layered double hydroxides and their decomposition products. Mater Chem Phys 75:19–25
32. Miyata S (1975) The syntheses of hydrotalcite-like compounds and their structures and physico-chemical properties I: the systems Mg^{2+}–Al^{3+}–NO_3^-, Mg^{2+}–Al^{3+}–ClO_4^-, Ni^{2+}–Al^{3+}–Cl^- and Zn^{2+}–Al^{3+}–Cl^-. Clay Clay Miner 23:369–375
33. Han KS, Guerlou-Demourgues L, Delmas C (1996) A new metavanadate inserted layered double hydroxide prepared by 'chimie douce'. Solid State Ionics 84:227–238
34. Menetrier M, Han KS, Guerlou-Demourgues L, Delmas C (1997) Vanadate-inserted layered double hydroxides: a V-51 NMR investigation on the grafting process. Inorg Chem 36:2441–2445
35. Imamura S, Sasaki H, Shono M, Kanai H (1998) Structure of molybdenum supported on alpha-, gamma-, and chi-aluminas in relation to its epoxidation activity. J Catal 177:72–81
36. Nakamoto K (2009) Infrared and Raman Spectra of Inorganic and Coordination Compounds Theory and Applications in Inorganic Chemistry, 6th edn. Wiley, New York
37. Liu Z, Chen Y (1998) Spectroscopic studies on tetragonal ZrO_2-supported MoO_3 and NiO-MoO_3 systems. J Catal 177:314–324
38. Faro AC, Grange P, dos Santos ACB (2002) Niobia-supported nickel molybdenum catalysts: Characterisation on the oxide form. Phys Chem Chem Phys 4:3997–4007
39. Carriazo D, Domingo C, Martin C, Rives V (2006) Structural and texture evolution with temperature of layered double hydroxides intercalated with paramolybdate anions. Inorg Chem 45:1243–1251
40. Corma A, Fornes V, Martin-Aranda MR, Rey F (1992) Determination of base properties of hydrotalcites: condensation of benzaldehyde with ethyl acetoacetate. J Catal 134:58–65